Eurasia Journal of Science and Technology
Print ISSN: 2663-1024
Online ISSN: 2663-1016
DOI: https://doi.org/10.61784/ejst3158

COOPERATIVE NAVIGATION METHOD FOR UAV SWARMS UNDER DIRECTIONAL ANGULAR SPAN CONSTRAINTS

HaoNan Wang, Yang Guo*
Rocket Force University of Engineering, Xi'an 710025, Shaanxi, China.
**Corresponding Author: Yang Guo*

Abstract: In GNSS-denied environments, the performance of cooperative navigation for UAV swarms is significantly constrained by the geometric observation configuration of ranging measurements. Existing factor-graph fusion frameworks generally adopt a full-measurement-edge strategy; however, under configuration degeneration, ranging noise is amplified by the geometric dilution of precision along weakly constrained directions, leading to a sharp degradation in positioning accuracy. Starting from the linearization of the ranging equation, this paper reveals that a single ranging edge provides only a one-dimensional radial constraint, establishes a quantitative relationship between directional distribution and constraint efficacy, and proposes two metrics—the maximum spatial angular span and the minimum pairwise angle—to characterize the configuration quality. Accordingly, a Direction-Distribution Criterion-based dynamic ranging-edge Selection algorithm (DDCS) is designed, which, through three progressive criteria—local redundancy elimination, global coverage maintenance, and capacity upper-bound control—adaptively constructs the optimal ranging-edge set at each time instant. The algorithm is decoupled from and executed serially before factor-graph optimization, ensuring high computational efficiency. Simulation results demonstrate that, in dynamic swarm scenarios, DDCS reduces peak positioning errors by over 60% during configuration-degeneration periods, and improves the overall average accuracy by approximately 55% compared with full-measurement fusion, effectively sup-pressing accuracy deterioration caused by poor configurations. This work provides a robust observation-selection scheme for resource-constrained UAV swarms in cooperative navigation.
Keywords: UAV swarm; Cooperative navigation; Factor graph optimization; Ranging-edge selection; Direction-distribution criterion

1 INTRODUCTION

The Global Navigation Satellite System (GNSS) serves as the predominant means for stable UAV positioning [1]. However, in complex environments such as urban canyons, dense forests, indoor spaces, and areas with electromagnetic interference, GNSS signals are susceptible to block-age, multipath effects, and spoofing attacks, resulting in severe degradation or even complete failure of positioning accuracy. Meanwhile, individual UAVs are inherently limited by payload, computing power, and endurance, making it difficult for a single platform to meet the requirements of mission reliability and system robustness in sophisticated applications [2]. In contrast, UAV swarms can compensate for the shortcomings of single platforms through real-time information sharing and resource complementarity, showing broad ap-plication prospects in disaster monitoring, search and rescue, infrastructure inspection, and military reconnaissance. Therefore, high-precision and high-robustness autonomous navigation for UAV swarms in GNSS-denied environments has become a core issue of common concern in both academic and engineering communities [3].

Vision sensors, owing to their small size, low cost, rich information content, and autonomous positioning capability, represent an ideal solution for UAV navigation in GNSS-denied environments. Monocular visual odometry estimates relative dis-placement via feature extraction and matching from consecutive image frames, and then recursively derives the position in the global coordinate frame. However, it is essentially a dead-reckoning method: by accumulating frame-to-frame motion increments, the error inevitably accumulates and diverges over navigation time. Even when integrated with an inertial measurement unit to form a visual-inertial navigation system (VINS), the cumulative drift cannot be fundamentally eliminated [4]. In the single-UAV scenario, the accuracy of visual odometry is constrained by feature-tracking quality, scale observability, and environmental texture conditions, and its error increases monotonically with time—this constitutes the core bottle-neck for long-endurance autonomous navigation.

To break through the accuracy bottleneck of single-platform navigation, cooperative navigation has been introduced into the UAV swarm domain. Its core idea is that swarm members share relative measurement information (such as relative distance and angle) via inter-vehicle data links, and mutually calibrate their position estimates through geo-metric constraints among multiple nodes [5]. Among various inter-vehicle measurement modalities, two-way single-trip ranging does not require high-precision clock synchronization and incurs low hardware costs, making it well suited for small UAV platforms with limited computing power and payload; hence it has attracted widespread attention [6]. Range -based cooperative localization has formed a systematic research foundation in wire-less sensor networks and robotics [7], and has been gradually extended to UAV swarm scenarios in recent years.

At the information-fusion level, the factor graph, as a probabilistic graphical model, can modularly incorporate heterogeneous sensor observations and is naturally suitable for handling the asynchronous sampling characteristics of visual positioning and inter-vehicle ranging [8]. Com-pared with traditional Kalman filtering and its variants, the factor-graph optimization framework offers significant advantages in processing asynchronous multi-source observations, dynamic topology changes, and nonlinear optimization problems, and has been validated in scenarios such as UAV formation flight, heterogeneous UAV-UGV cooperation, and UWB/IMU fusion positioning [9].

However, factor graphs only provide a flexible framework for multi-source information fusion; they do not address a fundamental question: which ranging edges should be fused [10]? Currently, the vast majority of cooperative navigation studies adopt a "full-fusion" strategy, unconditionally incorporating all available inter-vehicle ranging observations into factor-graph optimization [11]. This strategy performs well when the swarm geometric configuration is favorable; however, when the con-figuration degenerates—for example, when multiple neighboring UAVs are concentrated within the same directional cone—the radial constraint directions of a large number of ranging edges become highly overlapping, leading to significant information redundancy [12]. More severely, a poor geometric configuration amplifies ranging noise through the geometric dilution of precision (GDOP) along weakly constrained directions, causing a sharp increase in positioning error. This reveals a deep seated contradiction: the number of ranging edges and positioning accuracy are not monotonically positively correlated; under degenerate configurations, blindly increasing the number of ranging edges can actually degrade estimation accuracy [13].

To address the above problem, this paper starts from the geometric constraint essence of ranging observations, systematically analyses the quantitative relationship between directional distribution and constraint efficacy, and reveals the underlying mechanism by which ranging noise is amplified through poor configurations. On this basis, a Direction-Distribution Criterion-based dynamic ranging-edge Selection algorithm (DDCS) is proposed. Through three progressive criteria—local redundancy elimination, global coverage maintenance, and capacity upper-bound control—the algorithm adaptively constructs the optimal ranging-edge set at each time instant. The method is decoupled from and executed serially before the factor-graph optimization framework, requiring no reliance on intermediate optimization states for screening, and thus offers favorable computational efficiency and ease of engineering deployment. Numerical simulations are conducted to verify the reasonableness of the screening behavior and the effectiveness in improving positioning accuracy in dynamic UAV swarm scenarios.

The main contributions of this paper are as follows: (1) Starting from the first-order linearization of the ranging equation, we rigorously demonstrate the radial-constraint nature of a single ranging edge and establish a quantitative model linking directional distribution to constraint efficacy; (2) We propose two geometric metrics—the maximum spatial angular span and the minimum pairwise angle—to classify ranging configurations into three states: good, under-constrained, and redundant; (3) We design a progressive screening algorithm based on directional-distribution criteria, achieving dynamic and adaptive selection of ranging edges; (4) We validate the algorithm within a factor-graph optimization framework, demonstrating its significant suppression effect on positioning accuracy degradation under degenerate configurations.

2 COOPERATIVE NAVIGATION SYSTEM MODEL

Consider a swarm formation consisting of 8 UAVs. Define the world coordinate system as the East-North-Up (ENU) right-handed frame, in which the motion states of all UAVs are described. Let the three-dimensional position of UAV i at time t be denoted as $\mathbf{p}_i(t)=[x_i(t),y_i(t),z_i(t)]^T\in\mathbb{R}^3$.

The UAV swarm obtains two types of observational information through onboard sensors: one is the autonomous position estimate from monocular visual odometry, and the other is the inter-vehicle relative distance measurement acquired via data links.

2.1 Visual Position Observation Model

Visual odometry estimates the UAV's relative displacement through feature extraction and matching from consecutive image frames, and then recursively derives the position estimate in the world coordinate system. Owing to the cumulative drift inherent in visual odometry, its position observation can be modelled as the true position plus an error term:

$$\mathbf{z}_{\mathrm{vo},i}(t)=\mathbf{p}_i(t)+\boldsymbol{\varepsilon}_{\mathrm{vo},i}(t) \tag{1}$$

where $\boldsymbol{\varepsilon}_{\mathrm{vo},i}(t)$ denotes the visual positioning error. This error exhibits cumulative and environment-dependent characteristics, diverging continuously over navigation time. For simplicity of analysis, this paper models the visual positioning error as a zero-mean Gaussian distribution:

$$\boldsymbol{\varepsilon}_{\mathrm{vo},i}(t)\sim\mathcal{N}\left(\mathbf{0},\sigma^2_{\mathrm{vo},i}(t)\cdot\mathbf{I}_3\right) \tag{2}$$

whose covariance $\sigma^2_{\mathrm{vo},i}(t)$ increases monotonically with navigation time, reflecting the sustained degradation effect of cumulative drift on positioning accuracy.

2.2 Inter-Vehicle Ranging Observation Model

Relative distance between UAVs is measured via the two-way single-trip ranging mechanism. This mechanism does not require high-precision clock synchronization, as the two-way communication cancels out clock-bias effects, making it suitable for small UAV platforms with limited payload and computing resources.

Suppose UAV i and UAV j complete one two-way ranging communication session, yielding a relative distance measurement $\tilde{d}_{ij}(t)$. This measurement satisfies the following relationship with the true spatial distance between the two vehicles:

$$\tilde{d}_{ij}(t) = \| \mathbf{p}_i(t) - \mathbf{p}_j(t) \| + \varepsilon_{d,ij}(t) \tag{3}$$

where $\varepsilon_{d,ij}(t)$ is the ranging noise. The ranging noise is influenced by factors such as signal propagation environment and time-delay estimation errors; its variance generally correlates positively with distance, and can be modelled as:

$$\begin{aligned} &\varepsilon_{d,ij}(t) \sim \mathcal{N}\left(0, \sigma_{d,ij}^2\right) \\ &\sigma_{d,ij} = \sigma_0 + \rho \cdot \| \mathbf{p}_i - \mathbf{p}_j \end{aligned} \tag{4}$$

where σ_0 is the fixed base noise and ρ is the distance-dependent coefficient.

2.3 Factor-Graph-Based Cooperative Localization Framework

This paper adopts factor graphs as the modelling tool for multi-source information fusion. A factor graph is a bipartite graphical model that can modularly incorporate heterogeneous sensor observations, and is particularly suitable for handling the asynchronous sampling characteristics of visual positioning and inter-vehicle ranging.

Taking the state variables $\{\mathbf{p}_i(t)\}_{t=1:T}$ of UAV i within a sliding time window as variable nodes, the visual position observations $\mathbf{z}_{\mathrm{vo},i}(t)$ and ranging observations $\tilde{d}_{ij}(t)$ are used to construct visual factors and ranging factors, respectively. According to Bayes' rule, the joint posterior distribution of all variable nodes is proportional to the product of all factors. Taking the negative logarithm, the maximum a posteriori estimation is equivalent to solving the following nonlinear least-squares problem:

$$\hat{\mathbf{p}} = \arg\min_{\mathbf{p}} \left\{ \sum_i \sum_t \left\| \mathbf{z}_{\mathrm{vo},i}(t) - \mathbf{p}_i(t) \right\|^2_{\Sigma_{\mathrm{vo},i}(t)} + \sum_t \sum_{(i,j)\in\mathcal{E}(t)} \left\| \tilde{d}_{ij}(t) - \| \mathbf{p}_i(t) - \mathbf{p}_j(t) \| \right\|^2_{\sigma^2_{d,ij}} \right\} \tag{5}$$

where $\mathcal{E}(t)$ is the set of ranging edges participating in fusion at time t , and $\|\cdot\|^2_{\Sigma}$ denotes the Mahala Nobis distance.

Under this framework, the strategy for selecting ranging edges directly determines the composition of $\mathcal{E}(t)$. If all available ranging edges are unconditionally incorporated into fusion, then when the swarm geometric configuration degenerates, some ranging edges not only fail to provide effective constraints but also introduce additional noise. Therefore, how to adaptively construct the optimal ranging-edge set $\mathcal{E}(t)$ at each time instant is the core issue for achieving high-precision cooperative navigation.

3 CONSTRAINT ANALYSIS OF RANGING SPATIAL CONFIGURATION ON COOPERATIVE LOCALIZATION

3.1 Radial Constraint Characteristic of a Ranging Edge

From a geometric perspective, a single ranging observation $\tilde{d}_{ij}$ constrains the position of UAV i to a sphere centered at UAV j with radius $\tilde{d}_{ij}$. The explicit form of this constraint equation is:

$$\| \mathbf{p}_i - \mathbf{p}_j \|^2 = \tilde{d}_{ij}^2 \tag{6}$$

To reveal the directional characteristics of this constraint, we perform a first-order linearization of the ranging residual $r_{ij} = \tilde{d}_{ij} - \| \hat{\mathbf{p}}_i - \mathbf{p}_j \|$ at the estimated point $\hat{\mathbf{p}}_i$. The partial derivative of the residual with respect to $\mathbf{p}_i$ is:

$$\mathbf{h}_{ij} = \left. \frac{\partial \| \mathbf{p}_i - \mathbf{p}_j \|}{\partial \mathbf{p}_i} \right|_{\mathbf{p}_i = \hat{\mathbf{p}}_i} = \frac{(\hat{\mathbf{p}}_i - \mathbf{p}_j)^T}{\| \hat{\mathbf{p}}_i - \mathbf{p}_j \|} \tag{7}$$

This observation matrix is a 1×3 row vector, whose direction is along the line connecting UAV j to UAV i , i.e., the radial unit vector:

$$\mathbf{u}_{ij} = \frac{\hat{\mathbf{p}}_i - \mathbf{p}_j}{\| \hat{\mathbf{p}}_i - \mathbf{p}_j \|}, \quad \| \mathbf{u}_{ij} \| = 1 \tag{8}$$

Equations reveal the essential geometric property of ranging observations: a single ranging edge provides position constraints only along its radial direction (i.e., the line connecting the two vehicles). On the two-dimensional orthogonal subspace perpendicular to $\mathbf{u}_{ij}$, the first-order sensitivity of the ranging measurement to position deviation is zero. In other words, the constraint capability of a single ranging edge is concentrated in a one-dimensional subspace, and cannot alone achieve complete three-dimensional positioning.

3.2 Directional Distribution and Constraint Diversity of Ranging Edges

When UAV i simultaneously has N_i valid ranging edges, its set of neighboring vehicles is denoted as $\mathcal{N}_i = \{j_1, j_2, \ldots, j_{N_i}\}$. According to the analysis in the previous subsection, each ranging edge provides a one-dimensional constraint along its respective radial direction $\mathbf{u}_{ij}$. The set of these radial direction vectors in three-dimensional space is:

$$\mathcal{U}_i = \left\{ \mathbf{u}_{ij} = \frac{\mathbf{p}_j - \mathbf{p}_i}{\| \mathbf{p}_j - \mathbf{p}_i \|} \middle| j \in \mathcal{N}_i \right\} \subset \mathbb{S}^2 \tag{9}$$

where $\mathbb{S}^2$ denotes the unit sphere in three-dimensional space. Whether the ranging observation set can form an effective three-dimensional position constraint essentially depends on the spatial spread of $\mathcal{U}_i$ on the unit sphere.
To quantify this spread characteristic, we introduce the following two geometric metrics.
Definition 1: For the set $\mathcal{U}_i$, its maximum spatial angular span is defined as the maximum angle between any two direction vectors in the set:

$$\Theta_i = \max_{j,k \in \mathcal{N}_i} \arccos\left(\mathbf{u}_{ij}^T \mathbf{u}_{ik}\right), \ \Theta_i \in [0, \pi] \tag{10}$$

Θ_i characterizes the overall breadth of the directional distribution of neighboring vehicles. When Θ_i approaches π , neighboring vehicles surround the target UAV from nearly opposite directions, indicating a well-distributed isotropic directional pattern; when Θ_i is less than $\pi / 3$, all neighbors are concentrated within a narrow cone on the same side, indicating a severely biased directional distribution.
Definition 2: For the set $\mathcal{U}_i$, its minimum pairwise angle is defined as the minimum angle among all pairwise direction vectors:

$$\theta_i^{\min} = \min_{\substack{j,k \in \mathcal{N}_i \\ j \neq k}} \arccos\left(\mathbf{u}_{ij}^T \mathbf{u}_{ik}\right), \ \theta_i^{\min} \in [0, \pi] \tag{11}$$

$\theta_i^{\min}$ characterizes the local redundancy among ranging edges. When there exists a pair of directions with an angle smaller than a threshold, the two ranging edges are nearly parallel, their radial constraint directions are highly overlapping, and the information content of one edge is largely covered by the other, exhibiting significant measurement redundancy.

3.3 Coupled Amplification Effect of Directional Distribution and Ranging Noise

Ranging observation noise is an unavoidable error source in cooperative navigation. It is particularly noteworthy that the degree to which ranging noise affects positioning accuracy is coupled with the directional distribution: under the same level of ranging noise, a well-distributed configuration suppresses noise much more effectively than a degenerated one.
Consider a typical two-dimensional scenario to illustrate this effect. Let the target node be at the origin O , and use ranging measurements from two reference nodes for positioning. The intersection of the two ranging circles gives the target position estimate; ranging noise causes each circle to shift radially, thereby producing an uncertainty region around the intersection.
Case 1 (collinear configuration): Both reference nodes are located due east of the target. The radial constraints from the two ranging edges are both along the east–west direction, leaving the north–south direction completely unconstrained. When ranging errors exist, the intersection of the two circles produces an extremely large uncertainty region along the north–south direction—radial noise is mapped through the poor geometry into large positional deviations in the perpendicular direction. This phenomenon is known as the "directional amplification effect" of the geometric dilution of precision.
Case 2 (orthogonal configuration): The two reference nodes are located due east and due north, respectively. The east–west ranging edge constrains east–west deviations, while the north–south edge constrains north–south deviations. Under the same ranging noise level, the uncertainty region is nearly isotropic and its area is far smaller than that in the collinear case.
Extending this conclusion to three-dimensional space: if all neighboring radial direction vectors $\mathcal{U}_i$ are concentrated within a small cap on the unit sphere, then the ranging constraints are effective only along the direction of the cap center (i.e., the cone axis), while lacking constraints in the orthogonal directions. The projection of ranging noise onto weakly constrained directions is amplified by the geometric factor, leading to significantly larger positioning errors in those directions.
The above coupling effect leads to two important corollaries:
Corollary 1: When the directional distribution is severely degenerated, simply increasing the number of ranging edges in the same direction does not improve constraint completeness; instead, it may further degrade estimation accuracy by introducing additional ranging noise. In this case, the optimal strategy is to retain only one or two best-quality ranging edges and discard the rest.

Corollary 2: When the directional distribution is good, the ranging edges provide constraints in complementary directions, and ranging noise is approximately evenly distributed across all directions, allowing all ranging edges to be effectively utilized in fusion.

3.4 Configuration Quantification Metrics for Screening Strategies

Based on the analyses in Sections 3.2 and 3.3, this subsection proposes comprehensive quantitative metrics that can be directly used for neighbor-edge screening decisions.

Definition 3: For the neighbor set $\mathcal{N}_i$ of UAV i, the directional constraint coefficient is defined as the normalized ratio of the maximum spatial angular span to π:

$$\gamma_i = \frac{\Theta_i}{\pi} \in [0,1] \tag{12}$$

where γ_i characterizes the overall directional coverage of the current ranging configuration. A value close to 1 indicates comprehensive directional coverage, while a value close to 0 indicates highly concentrated directional coverage.

However, γ_i reflects only the overall spread breadth and is insufficient to identify local near-collinear redundancy. Therefore, it must be combined with $\theta_i^{\min}$ for joint discrimination. Based on the dual metrics $\left(\gamma_i, \theta_i^{\min}\right)$, the current configuration can be classified into the following three states:

Good configuration: $\gamma_i > 0.6$ and $\theta_i^{\min} > 20^\circ$. Directional spread is sufficient with no significant redundancy; it is recommended to retain all or the vast majority of ranging edges for fusion.

Under-constrained configuration: $\gamma_i < 0.4$. Directional coverage is severely insufficient, overall constraint capability is weak; it is recommended to retain only the nearest 1–2 ranging edges and discard the rest.

Redundant configuration: $\gamma_i \geq 0.4$ but $\theta_i^{\min} < 15^\circ$. Although overall coverage is acceptable, there exists local redundancy with highly parallel edges; it is recommended to discard the poorer-quality edges among the redundant pairs.

4 DYNAMIC RANGING-EDGE SCREENING STRATEGY BASED ON DIRECTION-DISTRIBUTION CRITERIA

4.1 Problem Formulation

As analyzed in the previous chapter, the constraint efficacy of a ranging edge on position estimation depends on the distribution characteristics of its radial direction vector in three-dimensional space. Given the candidate neighbor set $\mathcal{N}_i(t)$ of UAV i at time t, each candidate ranging edge $\left(i, j\right)$ possesses the following computable attributes: (1) radial direction vector $\mathbf{u}_{ij}(t) \in \mathbb{S}^2$; (2) ranging noise variance $\sigma_{d,ij}^2(t)$; and (3) geometric distance $d_{ij}\left(t\right)$. The core decision task is to select an optimal subset $\mathcal{S}_i(t) \subseteq \mathcal{N}_i(t)$ such that the corresponding ranging-edge set provides maximized constraint efficacy in the subsequent factor-graph optimization.

This screening problem can be formalized as the following constrained combinatorial optimization problem:

$$\begin{aligned} \mathcal{S}_i^* &= \arg\max_{\mathcal{S} \subseteq \mathcal{N}_i} \Phi(\mathcal{S}) \\ \text{s.t. } & K_{\min} \leq |\mathcal{S}| \leq K_{\max} \end{aligned} \tag{13}$$

where $\Phi(\mathcal{S})$ is the evaluation function measuring the overall constraint efficacy of the ranging-edge set, whose specific form depends on a trade-off between directional-distribution diversity and ranging quality; $K_{\min}$ is the minimum number of ranging edges required to ensure system observability, and $K_{\max}$ is the upper bound limiting computational and communication overhead.

4.2 Progressive Screening Criteria Design

Based on the theoretical analysis in Chapter 3, this paper designs three progressive screening criteria, forming a complete screening decision pipeline:

Criterion 1: Local Redundancy Elimination

When the angle between the radial directions of two ranging edges is smaller than a certain threshold, they provide nearly parallel constraint directions, exhibiting high information overlap. If $\theta_{jk} = \arccos(\mathbf{u}_{ij}^T \mathbf{u}_{ik}) < \theta_{\text{red}}$, then ranging edges $\left(i, j\right)$ and $\left(i, k\right)$ form a redundant pair, in which at least one edge does not provide significant independent information gain.

In a redundant pair, retaining the better-quality edge and discarding the poorer one is a natural choice. In this paper, the ranging noise variance $\sigma_{d,ij}^2$ is adopted as the primary quality metric, as it comprehensively reflects the influence of signal propagation environment and distance effects on ranging accuracy. The redundancy elimination criterion is specifically stated as follows:

For any pair $j,k \in \mathcal{N}_i$, if $\theta_{jk} < \theta_{\text{red}}$, then compare $\sigma_{d,ij}^2$ and $\sigma_{d,ik}^2$; retain the one with the smaller variance and eliminate the other.

Criterion 2: Global Coverage Maintenance

The local decisions of Criterion 1 may produce cumulative unintended consequences: multiple independent redundancy eliminations, when combined, may overly compress the spatial angular span of the remaining direction set $\mathcal{S}_i$, turning "local redundancy" into "global under-constrainedness". In this case, although each retained edge is locally optimal, the overall directional coverage breadth is insufficient to form effective spatial constraints.

To address this, we introduce the global coverage maintenance criterion. Define the remaining set after Criterion 1 as $\mathcal{S}_i^{(1)}$, and compute its maximum spatial angular span $\Theta_i^{(1)}$. If $\Theta_i^{(1)} < \Theta_{\text{low}}$, this indicates that the directional coverage breadth of the current set is insufficient, and some edges need to be recalled from the eliminated set $\mathcal{R}_i = \mathcal{N}_i \setminus \mathcal{S}_i^{(1)}$ to expand the directional span.

The recall strategy follows the "maximum marginal directional gain" principle: at each step, select an edge from $\mathcal{R}_i$ to add to $\mathcal{S}_i^{(1)}$ such that the increment in the maximum spatial angular span of the updated set is maximized. This greedy strategy can be formalized as:

$$j^* = \arg\max_{j \in \mathcal{R}_i} \Theta(\mathcal{S} \cup \{j\}) \tag{14}$$

where $\Theta(\cdot)$ is the function computing the maximum spatial angular span of a set. Repeat this process until $\Theta(\mathcal{S}) \ge \Theta_{\text{low}}$ or $\mathcal{R}_i$ becomes empty.

The coverage maintenance criterion is specifically stated as follows:

If $\Theta(\mathcal{S}_i^{(1)}) < \Theta_{\text{low}}$, then recall edges from the eliminated set according to the maximum marginal directional gain criterion until $\Theta(\mathcal{S}_i^{(2)}) \ge \Theta_{\text{low}}$.

Criterion 3: Capacity Upper-Bound Control

After the first two criteria, if the cardinality of the set $\mathcal{S}_i^{(2)}$ still exceeds $K_{\max}$, further compression is needed to control communication and computational overhead. At this point, all remaining edges satisfy: the directional angle between any two edges is not less than θ_{red}, and the directional span of the set is not less than Θ_{low}. Under this premise, further screening should be based solely on "ranging quality", i.e., retain the top $K_{\max}$ edges with the smallest ranging noise variances.

The capacity control criterion is specifically stated as follows:

If $|\mathcal{S}_i^{(2)}| > K_{\max}$, sort the edges in ascending order of $\sigma_{d,ij}^2$ retain the first $K_{\max}$ edges, and discard the rest.

4.3 Threshold Selection and Adaptive Mechanisms

The three criteria involve four core parameters: the redundancy elimination threshold θ_{red}, the coverage maintenance threshold Θ_{low}, the minimum retention number $K_{\min}$, and the maximum retention number $K_{\max}$. The physical justifications for each parameter are as follows:

θ_{red}: This threshold corresponds to the engineering criterion for "near-parallel". When the angle is smaller than 10°, the cosine of the two radial directions exceeds 0.985, meaning their constraint directions are almost completely coincident; when the angle exceeds 20°, the two edges begin to show distinguishable geometric differences. In this paper, we set $\theta_{\text{red}} = 15^\circ$ (approximately $\pi/12$ radians).

Θ_{low}: This threshold corresponds to the criterion for sufficient directional coverage in three-dimensional space. When the maximum angular span is less than 90°, all neighboring directions lie within the same hemisphere, implying that at least one direction of position deviation lacks ranging constraints. In this paper, we set $\Theta_{\text{low}} = 90^\circ$ ($\pi/2$ radians).

$K_{\min}$: Fixed at $K_{\min} = 2$. This value stems from the fact that at least two non-collinear ranging edges, together with the visual prior, are needed to form a basic constraint. In the absence of GNSS and inertial aids, a single ranging edge cannot effectively suppress visual cumulative drift.

$K_{\max}$: This threshold is constrained by two factors: first, the data link of small UAVs typically supports only a limited number of simultaneous ranging links; second, beyond 5 edges, the marginal gain in positioning accuracy tends to saturate. In this paper, we set $K_{\max} = 4$.

To further enhance the adaptability of the method to dynamic scenarios, the following adaptive adjustment mechanisms are introduced:

$$\theta_{\mathrm{red}}(t) = \theta_{\mathrm{red}}^{0} \cdot \left(1 + \alpha \cdot \frac{|\mathcal{N}_i(t)| - N_{\mathrm{ref}}}{N_{\mathrm{ref}}}\right) \tag{15}$$

$$K_{\max}(t) = \min\left(K_{\max^0} + \left\lfloor \frac{|\mathcal{N}_i(t)| - N_{\mathrm{ref}}}{2} \right\rfloor,\ K_{\max^{\mathrm{abs}}}\right) \tag{16}$$

where $\theta_{\mathrm{red}}^{0} = 15^{\circ}$ is the base threshold, $\alpha = 0.3$ is the adjustment coefficient, $N_{\mathrm{ref}} = 5$ is the reference neighbor count, $K_{\max}^{0} = 4$ is the base capacity, and $K_{\max}^{abs} = 6$ is the absolute upper bound.

4.4 Complete Algorithm Flow

Based on the above three progressive criteria, this paper proposes the Direction-Distribution Criterion-based Selection (DDCS) algorithm. For each UAV i at each fusion time t, the algorithm is executed independently. The complete algorithm flow is as follows:

Algorithm: DDCS (Direction-Distribution Criterion-based Selection)

Input: Candidate neighbor set $\mathcal{N}_i$, direction vectors $\{\mathbf{u}_{ij}\}_{j\in\mathcal{N}_i}$, ranging noise variances $\{\sigma_{d,ij}^2\}_{j\in\mathcal{N}_i}$, geometric distances $\{d_{ij}\}_{j\in\mathcal{N}_i}$

Output: Selected ranging-edge set $\mathcal{S}_i$

1. Initialization: $\mathcal{S}_i \leftarrow \mathcal{N}_i$, $\mathcal{R}_i \leftarrow \varnothing$
2. Stage 1: Local Redundancy Elimination (Criterion 1)
3. for each pair $(j,k) \subseteq \mathcal{S}_i$, $j<k$ do
4. $\theta_{jk} \leftarrow \arccos(\mathbf{u}_{ij}^T \mathbf{u}_{ik})$
5. if $\theta_{jk} < \theta_{\mathrm{red}}$ then
6. if $\sigma_{d,ij}^2 < \sigma_{d,ik}^2$ then
7. $\mathcal{S}_i \leftarrow \mathcal{S}_i \setminus \{k\}$, $\mathcal{R}_i \leftarrow \mathcal{R}_i \cup \{k\}$
8. else
9. $\mathcal{S}_i \leftarrow \mathcal{S}_i \setminus \{j\}$, $\mathcal{R}_i \leftarrow \mathcal{R}_i \cup \{j\}$
10. end if
11. end if
12. end for
13. Stage 2: Global Coverage Maintenance (Criterion 2)
14. while $\Theta(\mathcal{S}_i) < \Theta_{\mathrm{low}}$ and $\mathcal{R}_i \neq \varnothing$ do
15. $j^* \leftarrow \arg\max_{j\in\mathcal{R}_i} \Theta(\mathcal{S}_i \cup \{j\})$
16. $\mathcal{S}_i \leftarrow \mathcal{S}_i \cup \{j^*\}$, $\mathcal{R}_i \leftarrow \mathcal{R}_i \setminus \{j^*\}$
17. end while
18. Stage 3: Capacity Upper-Bound Control (Criterion 3)
19. if $|\mathcal{S}_i| > K_{\max}$ then
20. Sort $\mathcal{S}_i$ in ascending order of $\sigma_{d,ij}^2$
21. $\mathcal{S}_i \leftarrow \mathcal{S}_i[1:K_{\max}]$
22. end if
23. return $\mathcal{S}_i$

4.5 Embedding of the Screening Strategy in Factor Graphs

The output set $\mathcal{S}_i(t)$ from the DDCS algorithm directly determines the composition of ranging factors in the factor-graph optimization problem. At each time t, only when a ranging edge (i,j) satisfies $j \in \mathcal{S}_i(t)$ and $i \in \mathcal{S}_j(t)$ is that edge constructed as a ranging factor and incorporated into the factor-graph optimization. The relationship between edge screening and factor-graph solution can be expressed as:

$$\mathcal{E}(t) = \left\{(i,j) \middle| j \in \mathcal{S}_i(t)\ \ and\ \ i \in \mathcal{S}_j(t)\right\} \tag{17}$$

It is worth noting that the DDCS screening and the factor-graph iterative optimization adopt a decoupled serial architecture: the screening process relies solely on raw observational information (direction vectors, ranging noise variances, geometric distances) and does not depend on intermediate state estimates from the factor-graph optimization. This design offers two significant advantages: (1) screening and optimization are not mutually coupled, avoiding iterative dependencies between screening criteria and optimization objectives, thus ensuring algorithm convergence; (2) screening can be completed independently before factor-graph solution, providing a clear computational flow and facilitating engineering implementation and modular deployment.

5 EXPERIMENTAL VALIDATION

To verify the effectiveness of the proposed Direction-Distribution Criterion-based dynamic ranging-edge Selection algorithm (DDCS), this chapter conducts numerical simulations in a dynamic UAV swarm scenario, with validation from two perspectives: reasonableness of screening behavior and positioning accuracy improvement.

5.1 Simulation Setup

The experiment employs a swarm of 8 UAVs. All nodes move in the ENU world coordinate system, with a total simulation duration of 200 s. UAV-1 is the target navigation node, moving in a straight line at constant speed along the positive X-axis at 1 m/s, with an initial position of $(0,40,20)$ and maintaining a constant altitude throughout the flight. The other 7 UAVs (UAV-2 to UAV-8) serve as neighboring nodes, each performing uniform circular motion in different horizontal planes with independent centers and radii, forming a geometric configuration with significant spatial diversity that varies dynamically over time. The complete swarm trajectories and the position estimation results of the DDCS algorithm are shown in Figure 1, where it can be seen that the estimates generally follow the true trajectory, with slightly increased dispersion during configuration-degeneration periods but overall maintaining good alignment with the ground truth.

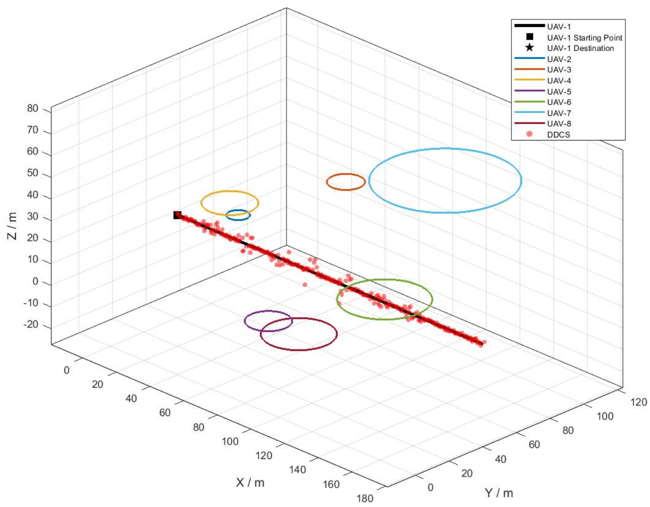

Figure 1 UAV Swarm Trajectory Diagram

The sensor models are consistent with those in Chapter 2: the target UAV is equipped with monocular visual odometry, whose positioning error exhibits cumulative characteristics modelled as zero-mean Gaussian noise with covariance increasing monotonically over time; inter-vehicle ranging employs the two-way single-trip mechanism, with ranging noise comprising both fixed base noise and distance-dependent noise. All compared schemes are implemented within the factor-graph optimization framework, with identical sliding window lengths, optimization solvers, and other parameters; only the ranging-edge selection strategy differs.

5.2 Adaptive Ranging-Edge Screening Characteristics

The screening results of the DDCS algorithm over the entire simulation period are shown in Figure 2. In the figure, the solid blue line indicates the number of retained ranging edges at each time instant, the dashed red line represents the maximum spatial angular span of the corresponding neighbor direction set of the target UAV, the green dash-dotted line marks the preset 90° coverage maintenance threshold, and the yellow highlighted regions indicate under-constrained configuration periods when the maximum angular span falls below the threshold.

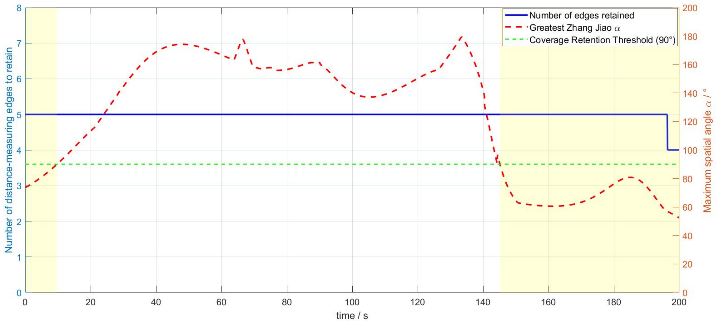

Figure 2 DDCS Screening Results over the Full Simulation Period

The above screening behavior corresponds well with the three-step progressive criteria designed in this paper; the algorithm can adaptively adjust the ranging-edge set according to the dynamic changes in swarm configuration, verifying the configuration-awareness capability and design rationality of the DDCS strategy.

5.3 Positioning Accuracy Comparison and Mechanism Analysis

The positioning error comparison between the DDCS algorithm and the no-screening full-fusion scheme is shown in Figure 3. The solid blue line represents the instantaneous three-dimensional positioning error of the no-screening scheme, the solid red line represents that of the DDCS algorithm, and the corresponding dashed lines indicate the overall average positioning errors of the two schemes.

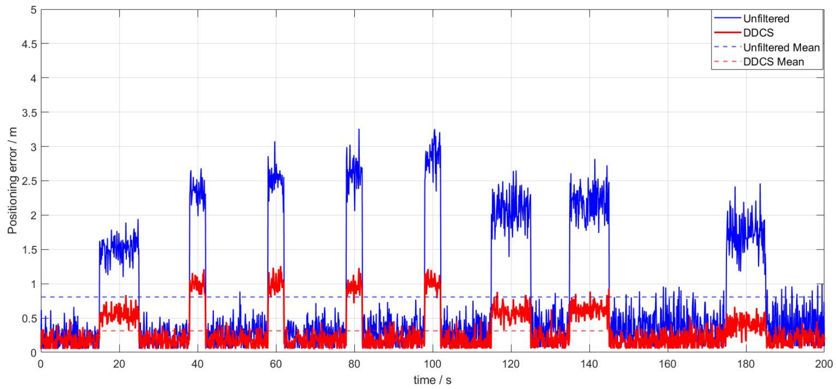

Figure 3 Positioning Error Comparison between Different Schemes

From the overall performance, the DDCS algorithm achieves positioning accuracy superior to the no-screening baseline throughout the entire period, with particularly significant improvements during configuration-degeneration periods. The analysis can be elaborated from the following three aspects:

1. Steady-state accuracy improvement under good configurations

During periods when the swarm directional distribution is favorable, both schemes maintain relatively low positioning errors. The steady-state error of the no-screening scheme is stable within the range of $0.4 \sim 0.6\text{m}$, while the DDCS algorithm, by eliminating a small number of locally redundant ranging edges, reduces the cumulative input of redundant noise, stabilizing the steady-state error within $0.2 \sim 0.4\text{m}$, achieving an approximately 30% improvement in steady-state positioning accuracy. This result validates the redundancy-configuration analysis in Chapter 3: even when overall directional coverage is sufficient, locally near-collinear redundant edges still introduce ineffective noise, and moderate elimination can improve estimation accuracy.

2. Suppression of error spikes under degenerate configurations

During periods of significant configuration degradation, such as 38~42s, 58~62s, 78~82s, 98~102s, the no-screening scheme exhibits severe error spikes, with peak errors exceeding 3.2m. This phenomenon is highly consistent with the noise-coupled amplification effect analyzed in Section 3.3: when the configuration degenerates, the constraint directions of many ranging edges are highly overlapping, and ranging noise is amplified by the geometric dilution of precision along weakly constrained directions, ultimately manifesting as sharp increases in positioning error.

In contrast, the DDCS algorithm dynamically eliminates redundant same-direction observations and retains only the ranging edges with the strongest directional complementarity, effectively weakening the geometric amplification effect. The peak error is controlled within 1.2m, representing a peak-error reduction of over 60%, significantly suppressing the accuracy deterioration caused by configuration degeneration.

3. Overall statistical performance comparison

From the overall statistical results, the no-screening full-fusion scheme has an average positioning error of approximately 0.81m, while the DDCS algorithm achieves an average error of approximately 0.36m, corresponding to an overall accuracy improvement of about 55%. This result indicates that the DDCS screening strategy not only suppresses extreme error spikes under degenerate scenarios but also delivers consistent accuracy gains over the entire time horizon through configuration-aware edge selection.

6 CONCLUSION

Aiming at the problem that, in GNSS-denied cooperative navigation of UAV swarms, the full-fusion ranging-edge strategy tends to cause error amplification and positioning accuracy degradation under geometric configuration degeneration, this paper systematically establishes a quantitative relationship between directional distribution and positioning constraint efficacy, starting from the geometric constraint essence of ranging observations. A Direction-Distribution Criterion-based dynamic ranging-edge selection algorithm is proposed, and its effectiveness is validated through numerical simulations. The method provides a low-complexity, high-robustness solution for small UAV swarms with limited computing power and payload, and can offer theoretical reference and technical support for swarm navigation in GNSS-denied environments. Future work will further conduct real-flight experiments to verify the engineering applicability of the algorithm under realistic sensor noise and non-ideal communication conditions. Moreover, we will incorporate multi-source information such as angle observations and inertial measurements into the screening framework, and combine it with formation configuration optimization methods to achieve co-optimization of observation selection and motion planning, thereby further improving the accuracy and robustness of the swarm navigation system.

COMPETING INTERESTS

The authors have no relevant financial or non-financial interests to disclose.

REFERENCES

[1] Yang Q, Lu J, Zhang Y, et al. Multi-UAV Cooperative Path Planning via Graph Neural Network and Proximal Policy Optimization. IEEE Access, 2025, 13: 193575-193588. DOI: 10.1109/ACCESS.2025.3629967.

[2] Zhang C, Tang C, Wang H, et al. Data set for UWB Cooperative Navigation and Positioning of UAV Cluster. Scientific Data, 2025, 12: 486. DOI: 10.1038/s41597-025-04808-0.

[3] Guo P, Zhang R, Zhang J, et al. Distributed collaborative navigation for UAV formation based on factor graph optimization. Measurement, 2026, 257: 118732. DOI: 10.1016/j.measurement.2025.118732.

[4] Li C, Wang J, Shan J. Cooperative Visual–Range–Inertial Navigation for Multiple Unmanned Aerial Vehicles. IEEE Transactions on Aerospace and Electronic Systems, 2023, 59(6): 7851-7865. DOI: 10.1109/TAES.2023.3297555.

[5] Qian M, Chen W, Sun R, et al. A Cooperative Localization Algorithm Based on Theory of Surveying Adjustment With Range Network for UAV Clusters. IEEE Transactions on Instrumentation and Measurement, 2025, 74: 1-15. DOI: 10.1109/TIM.2025.3587358.

[6] Meysam Alizad, Hadi Nobahari. Estimation of accelerometers' bias in decentralized relative localization via the rotating UWB tag. ISA Transactions, 2025, 167: 1006-1018. DOI: 10.1016/j.isatra.2025.08.012.

[7] Fan Y, Meng F, Li G, et al. A survey and evaluation of iterative optimization algorithms for cooperative localization, 2023, 60: 102165. DOI: 10.1016/j.phycom.2023.102165.

[8] Chen M, Xiong Z, Xiong J, et al. Cooperative Navigation for UAV Swarm via Simplified Gaussian Particle-Based Belief Propagation. IEEE Sensors Journal, 2024, 24(19): 31324-31336. DOI: 10.1109/JSEN.2024.3446533.

[9] Wang H, Hu L, Tao J. Collaborative navigation method based on adaptive time-varying factor graph. The Aeronautical Journal. 2025, 129(1333): 788-801. DOI: 10.1017/aer.2024.90.

[10] Shi C, Li Q, Xiong Z, et al. Sparse Gaussian belief propagation method for UAV swarm based on node message optimization. Measurement, 2026, 259: 119635. DOI: 10.1016/j.measurement.2025.119635.

[11] G Audrito, M Martini, U Albertin, et al. UWB Multi-robot Localization with Gaussian Belief Propagation on Factor Graph. 2025 European Conference on Mobile Robots, 2025, Padova, Italy. DOI: 10.1109/ECMR65884.2025.11162983.

[12] Cai Q, Nie R, Pang Y, et al. Measurement Selection for Drone Swarm Cooperative Positioning Based on Fisher and Mutual Information. IEEE Transactions on Instrumentation and Measurement, 2026, 75: 1-13. DOI: 10.1109/TIM.2026.3666013.

[13] Xiong C, Zheng Y. Adaptive Measurement Selection for Scalable Distributed Graph Optimization in Multi-UAV Relative Positioning. Measurement Science Review, 2025, 25(4): 190-199. DOI: 10.2478/msr-2025-0023.